Angewandte Chemie
Eine Zeitschrift der Gesellschaft Deutscher Chemiker

Supporting Information

Exploring the Formation of Black Phosphorus Intercalation Compounds with Alkali Metals

*Gonzalo Abellán, Christian Neiss, Vicent Lloret, Stefan Wild, Julio C. Chacón-Torres, Katharina Werbach, Filippo Fedi, Hidetsugu Shiozawa, Andreas Görling, Herwig Peterlik, Thomas Pichler, Frank Hauke, and Andreas Hirsch**

anie_201707462_sm_miscellaneous_information.pdf

Supporting Information

Exploring the Formation of Black Phosphorus Intercalation Compounds with Alkali Metals

Gonzalo Abellán, Christian Neiss, Vicent Lloret, Stefan Wild, Julio C. Chacón-Torres, Katharina Werbach, Filippo Fedi, Hidetsugu Shiozawa, Andreas Görling, Herwig Peterlik, Thomas Pichler, Frank Hauke and Andreas Hirsch*

1. Materials and Methods

Experimental Section.

Materials

BP crystals were purchased from Smart Elements (purity 99.998%); potassium, sodium and other chemicals were purchased from Chemicals and solvents were purchased from Sigma Aldrich Co. (Germany) and were used as received if not stated otherwise.

Sample preparation in the glove box

Sample preparation was carried out in different argon-filled Labmasterpro sp glovebox (MBraun), equipped with a gas purifier and solvent vapor removal unit, with an oxygen content <0.1 ppm and a water content <0.1 ppm. Firstly, we thoroughly grinded the BP crystals to obtain an homogeneous fine powder, then we mixed progressively the BP with stoichiometric amounts of the respective alkali metal in glass vials at controlled temperature. Once the materials were in close contact, the temperatures were slowly increased until 70 °C and 120 °C for Na and K, respectively. Finally, the samples were homogenized by a thermal treatment for *ca*. 24 h. at the corresponding temperatures. The samples were handled with extreme care avoiding mechanical agitation and using Teflon spatulas and tweezers.

For the entire study the samples were stored under conditions with water and oxygen contents of < 0.1 ppm.

Chemical composition

The chemical composition of the intercalated compounds was determined by energy dispersive X-ray spectroscopy (EDS) using an Oxford Instruments X-Max detector integrated with a focused ion beam/scanning electron microscope (FIB/SEM) FEI-Helios NanoLab 600i FIB Workstation).

According to the EDS mappings, the distribution of intercalated metal atoms is fairly uniform for all studied M_xP compounds (namely, 1:4, $X_{0.25}P$; 1:6, $X_{0.17}P$; and 1:8, $X_{0.125}P$). Our EDS analysis yielded the average concentrations of $K_{0.23}P$; $K_{0.18}P$, $K_{0.16}P$, for K and $Na_{0.27}P$; $Na_{0.17}P$; $Na_{0.14}P$, for Na intercalated crystals, respectively (typical error in these measurements was 5 at.%). Within this accuracy, we found that the concentrations correspond to the theoretical stoichiometric composition of monovalent alkali-metal intercalated BP.

Raman spectroscopy

Raman spectra were acquired on a LabRam HR Evolution confocal Raman microscope (Horiba) equipped with an automated XYZ table using 0.80 NA objectives. All measurements (unless otherwise noted) were conducted using an excitation wavelength of 532 nm, with an acquisition time of 2 s and a grating of 1800 grooves/mm. To minimize the photo-induced laser oxidation of the samples, the laser intensity was kept at 5 % (0.88 mW). The spectra were recorded in argon atmosphere (using a home-made sealed holder) using a green laser (λ_{exc}=532 nm). The step sizes in the Raman mappings used for the mean spectra were in the 0.5–1 µm range depending on the experiments. Data processing was performed using Lab Spec 5 as evaluation software.

In situ Raman spectroscopic detection was carried out inside a quartz tube through a flat (0.7 mm thick) optical window of borosilicate glass (PGO GmbH) in ultra-high vacuum chamber at ~4×10^{-8} mbar where the pristine BP was placed in a sample boat and the selected alkali metal in a vial. The Raman measurements were performed at room temperature using a Horiba LabRam spectrometer with a 514 nm excitation wavelength at 0.5 mW between 300 and 3,000 cm^{-1}. To avoid laser-induced damages the laser power was kept below 0.5 mW.

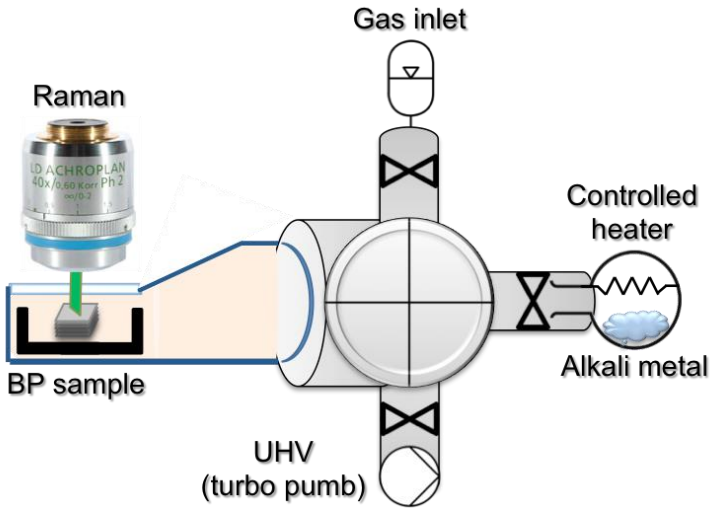

Fig. SI1: Schematic illustration of the setup for the controlled reaction of BP with alkali metals under ultra-high vacuum conditions. The reaction progress is monitored by *in situ* Raman spectroscopy.

XRD diffraction

XRD was performed by placing the material in the glove box (Labmasterpro sp glovebox; MBraun) into glass capillaries with 1 to 2 mm diameter and 10 micron wall thickness (from Hilgenberg). The capillaries were sealed with polymeric caps and then directly transported into the vacuum chamber of a microfocus X-ray device operating at a wavelength of 0.1542

nm, which is equipped with a 2D detector (VÅNTEC 2000) and an image plate system (Fujifilm FLA 7000) for simultaneous small-angle and wide-angle X-ray scattering. As the whole beamline operates in vacuum, background scattering from air is avoided. Finally, all two-dimensional X-ray patterns were radially averaged and additionally background corrected for pinhole and capillary scattering to obtain X-ray intensities in dependence on the scattering angle 2θ.

2. DFT calculations

Computational details

All calculations were performed employing a plane wave basis set within the PAW approach using the Vienna ab-inito Simulation Package (VASP 5.4).[1-4]

We applied the exchange-correlation density functional according to Perdew, Becke and Ernzerhof[5] (PBE) in connection with the Grimme D3 dispersion correction[6,7] (without Becke-Johnson damping) to properly account for van-der-Waals interactions. Geometry optimizations were considered converged when all residual force components (incl. the cell parameters) were smaller than 0.002 eV/Å, the SCF convergence criterion was at least 10^{-5} eV.

Atomic cores were modelled by the PAW potentials of VASP 5.4, leaving five / nine / seven electrons in the valence region of P / K /Na atoms, respectively. The plane wave cut-off energy was set to 300 eV throughout (except for Raman intensities, see below).

A Methfessel-Paxton smearing of first order with σ=0.1 eV was employed.[8] Final energies were evaluated extrapolating the total energies to $\sigma \rightarrow 0$. To sample the first Brillouin zone Monkhorst-Pack meshes (always shifted to Γ) were used.[9] The number of k-points was chosen such that a k-point distance of 0.02 – 0.01 2π/Å per reciprocal direction was obtained which leads to different k-point numbers for the different systems considered here.

All geometry optimizations were done assuming non-spinpolarized systems, low-energy structures were however re-checked for spin-polarization after geometry-optimization by performing spin-polarized single-point calculations, but in no case spin-polarization occurred.

Vibrational frequencies and normal modes were calculated at the Γ-point within the harmonic approximation.

A partially different setup was employed for the calculation of Raman intensities: the energy cut-off was set to 500 eV, a Gaussian smearing with σ=0.001 eV was used, and a very tight SCF convergence criterion of 10^{-8} eV was chosen.

Structure models of intercalation compounds / alloys

Structure models for crystalline potassium intercalation compounds with K:P $\leq$ 1:2 were obtained by successively putting metal atoms between the layers of pristine BP. For each of the intercalation compounds several different start configurations for geometry optimization were considered, i.e. by starting from different stacking modes between the BP sheets, and various distribution patterns of K atoms between the sheets. The corresponding sodium intercalation compounds were obtained by substituting K with Na in the optimized potassium intercalation structures.

For comparison also several other (known) K-P alloys were calculated: K_3P, K_4P_3, KP, K_2P_3, and K_3P_{11}. These structures were taken from the Materials Project data base [10] and subsequently re-optimized using the same methodology as for the intercalation compounds. They cannot be described as modified BP plus intercalated alkali atoms; therefore, we denote these structures as alloys.

Additional files:

POSCARs.zip

Optimized geometries of calculated K-P and Na-P structures bearing no imaginary frequencies at the Γ-point, in POSCAR format. The extrapolated total energy to $\sigma \rightarrow 0$ for every structure is stated in the first line of each POSCAR file.

Calculated band gaps

Compound	BP	KP_8	KP_4	KP_2	
Gap (eV)	0.0 (*)	0.0	0.0 (**)	1.25	
Compound	K_3P_{11}	K_2P_3	KP	K_4P_3	K_3P
Gap (eV)	1.82	0.69	1.11	0.0	0.28
Compound	NaP_8	NaP_4	Na_3P		
Gap (eV)	0.0	0.0	0.54		

Tab. SI1: Calculated band gaps of BP, the most stable intercalation compounds, and known structures using the PBE density functional. (*) band gap using the HSE06 density functional: 0.15 eV; (**) band gap using the HSE06 density functional: 0.0 eV

Computed reaction energies

Reaction	ΔE (eV)	ΔE per P atom (eV)
$4\ K_3P + P \rightarrow 3\ K_4P_3$	-4.835	-0.537
$K_4P_3 + P \rightarrow 4\ KP$	-0.805	-0.201
$2\ KP + P \rightarrow K_2P_3$	-0.494	-0.165
$K_2P_3 + P \rightarrow 2\ KP_2$	-0.200	-0.050
$3\ KP_2 + 5\ P \rightarrow K_3P_{11}$	-0.948	-0.086
$K_3P_{11} + P \rightarrow 3\ KP_4$	1.114	0.093
$KP_4 + 4\ P \rightarrow KP_8$	0.071	0.009

Tab. SI2: Computed reaction energies of K-P compounds with BP. For every stoichiometry the most stable compound was considered.

Reaction	ΔE (eV)	ΔE per P atom (eV)
$8\ P + K \rightarrow KP_8$	-1.175	-0.147
$KP_8 + K \rightarrow 2\ KP_4$	-1.318	-0.165
$11\ KP_4 + K \rightarrow 4\ K_3P_{11}$	-5.704	-0.130
$2\ K_3P_{11} + 5\ K \rightarrow 11\ KP_2$	-0.903	-0.150
$K_2P_3 + K \rightarrow 3\ KP$	-0.461	-0.154
$3\ KP + K \rightarrow K_4P_3$	-0.151	-0.050
$K_4P_3 + K \rightarrow 3\ K_3P$	-0.144	-0.048

Tab. SI3: Computed reaction energies of BP and K-P compounds with K. For every stoichiometry the most stable compound was considered.

3. Scanning electron microscopy and energy dispersive X-ray spectroscopy

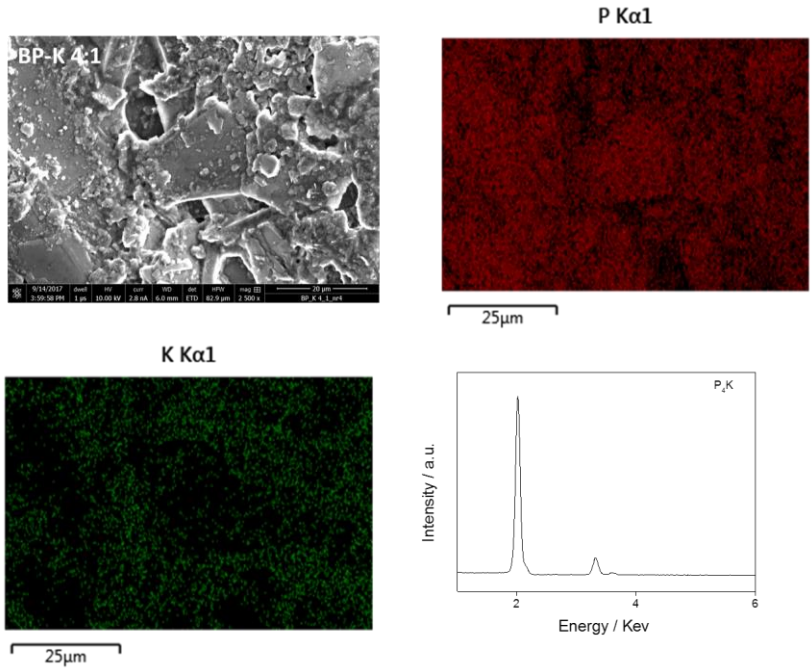

Fig. SI2: SEM image, EDS elemental maps and the corresponding energy dispersive X-ray spectra for K intercalated black phosphorus (BP-K 4:1).

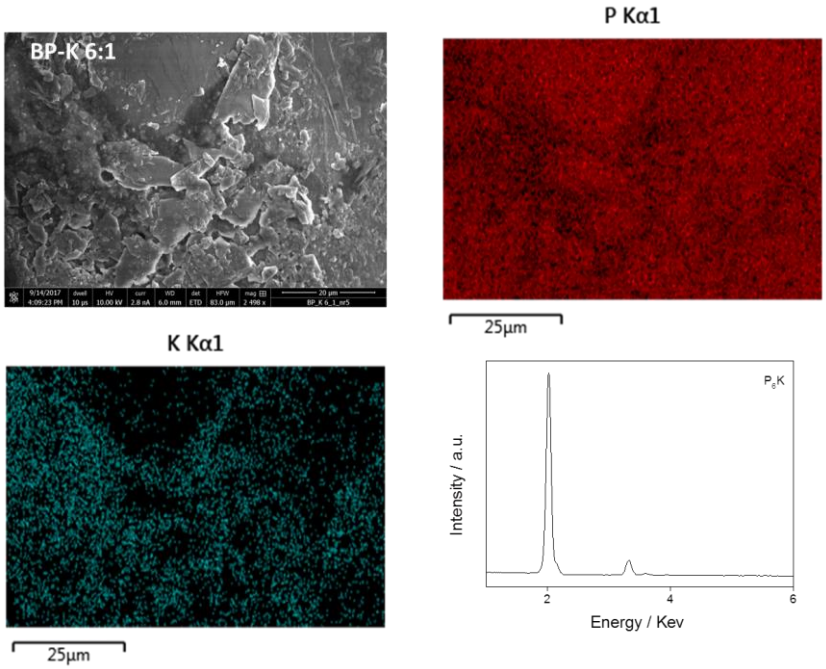

Fig. SI3: SEM image, EDS elemental maps and the corresponding energy dispersive X-ray spectra for K intercalated black phosphorus (BP-K 6:1).

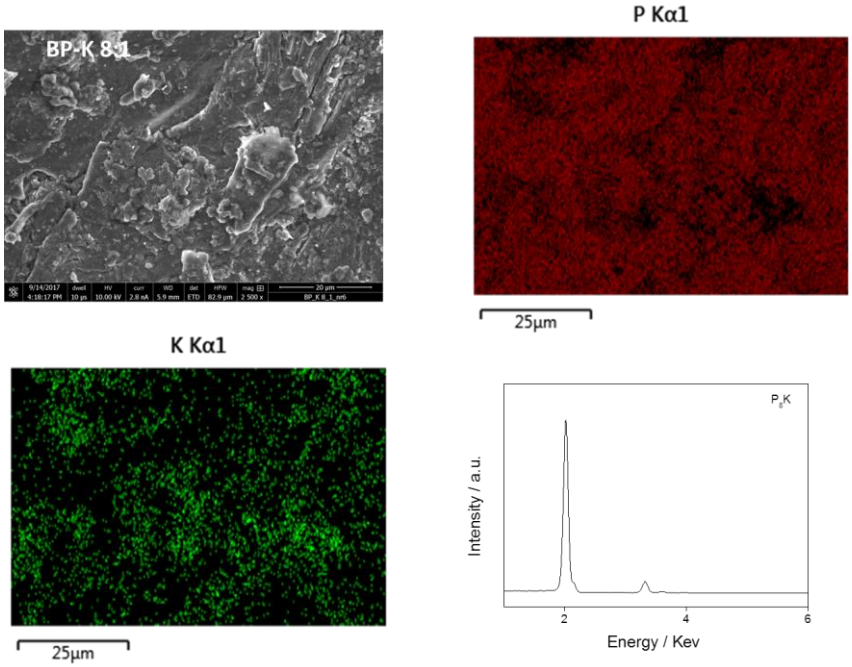

Fig. SI4: SEM image, EDS elemental maps and the corresponding energy dispersive X-ray spectra for K intercalated black phosphorus (BP-K 8:1).

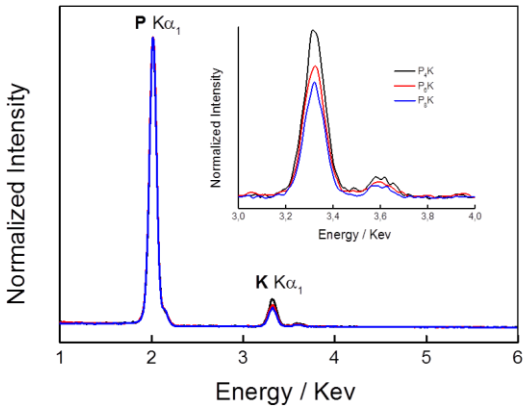

Sample	P	K
4:1	70.9	16.4
6:1	75.1	13.8
8:1	80.2	13.0

Fig. SI5: Comparative energy dispersive X-ray spectra and average composition for K intercalated black phosphorus samples.

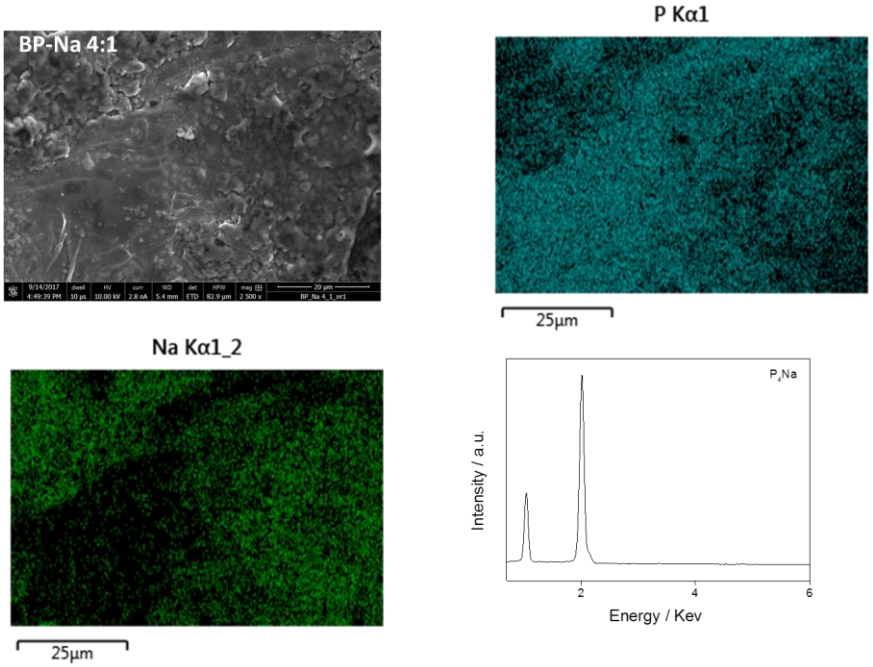

Fig. SI6: SEM image, EDS elemental maps and the corresponding energy dispersive X-ray spectra for Na intercalated black phosphorus (BP-Na 4:1).

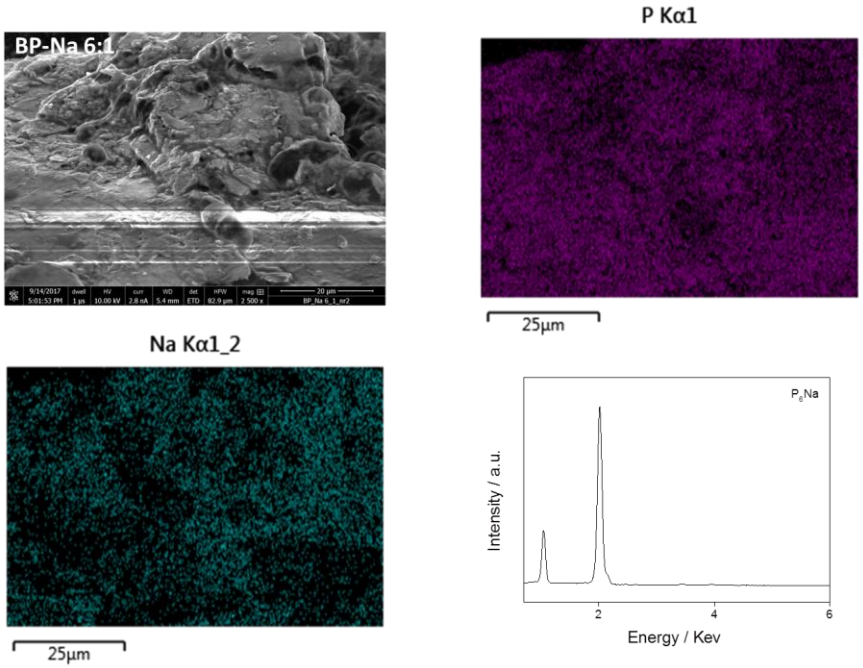

Fig. SI7: SEM image, EDS elemental maps and the corresponding energy dispersive X-ray spectra for Na intercalated black phosphorus (BP-Na 6:1).

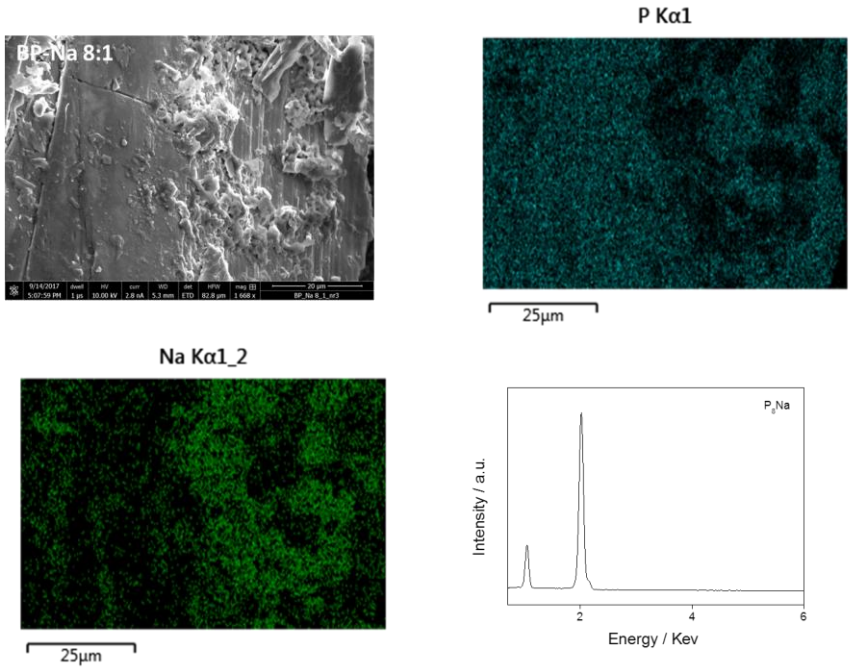

Fig. SI8: SEM image, EDS elemental maps and the corresponding energy dispersive X-ray spectra for Na intercalated black phosphorus (BP-Na 8:1).

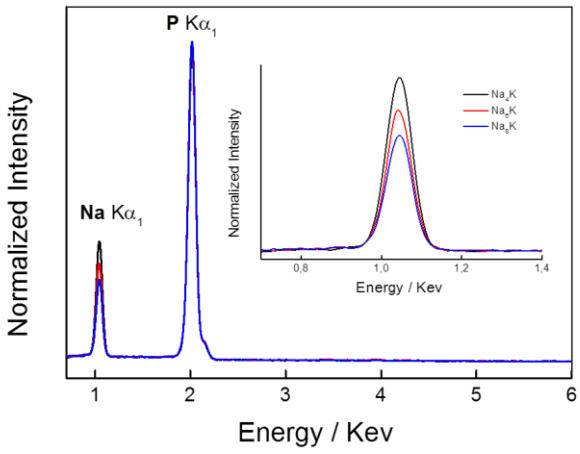

Sample	P	K
4:1	62.9	16.8
6:1	68.9	12.0
8:1	73.9	10.3

Fig. SI9: Comparative energy dispersive X-ray spectra and average composition for Na intercalated black phosphorus samples.

4. X-ray diffraction experiments

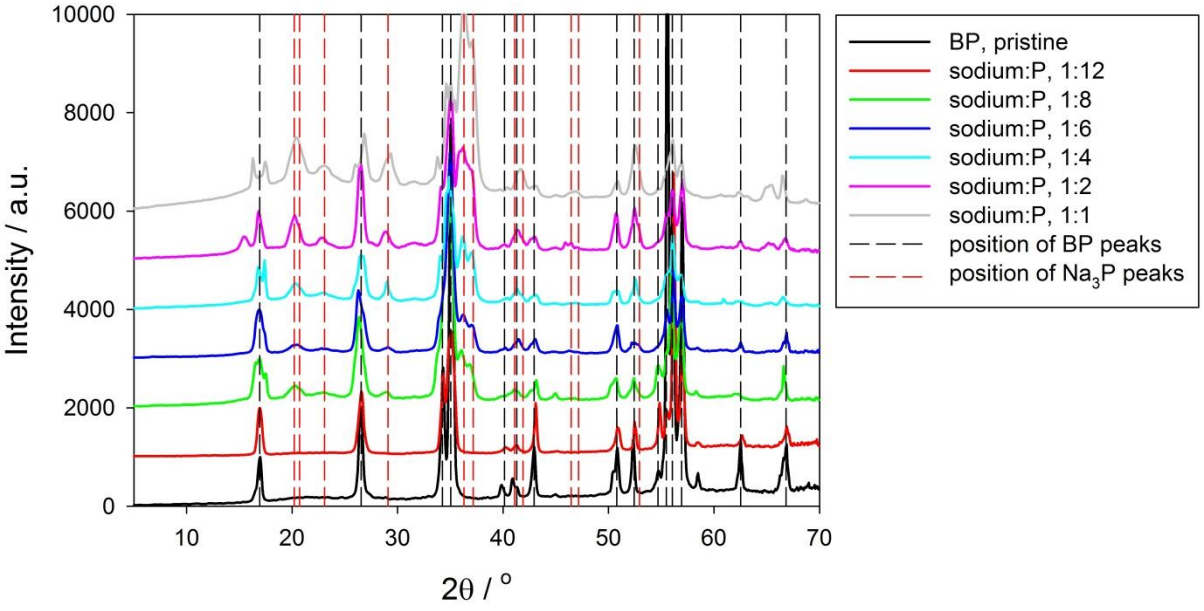

Fig. SI10: X-ray intensities for sodium@BP vs. scattering angle 2θ, with capillary and amorphous background subtracted. X-ray intensities are vertically shifted for better visibility. Black dashed lines indicate peak positions from BP, red dashed lines from Na_3P. Visible is e.g. a splitting/broadening of the first peak at a scattering angle of about 2θ=16° (and also of some higher order peaks) as well as an increasing intensity of peaks arising from crystalline Na_3P.

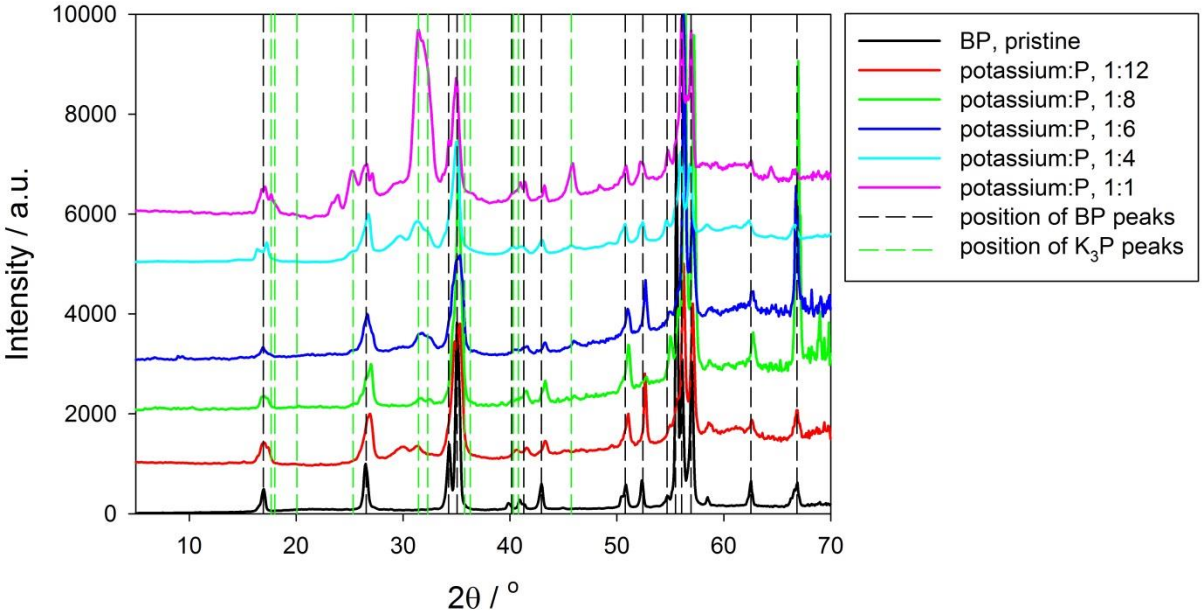

Fig. SI11: X-ray intensities for potassium@BP vs. scattering angle 2θ, with capillary and amorphous background subtracted. X-ray intensities are vertically shifted for better visibility. Black dashed lines indicate peak positions from BP, red dashed lines peaks from K_3P. Visible is e.g. a splitting/broadening of the first peak at a scattering angle of about 2θ=16° (and also of some higher order peaks) as well as an increasing intensity of peaks arising from crystalline K_3P.

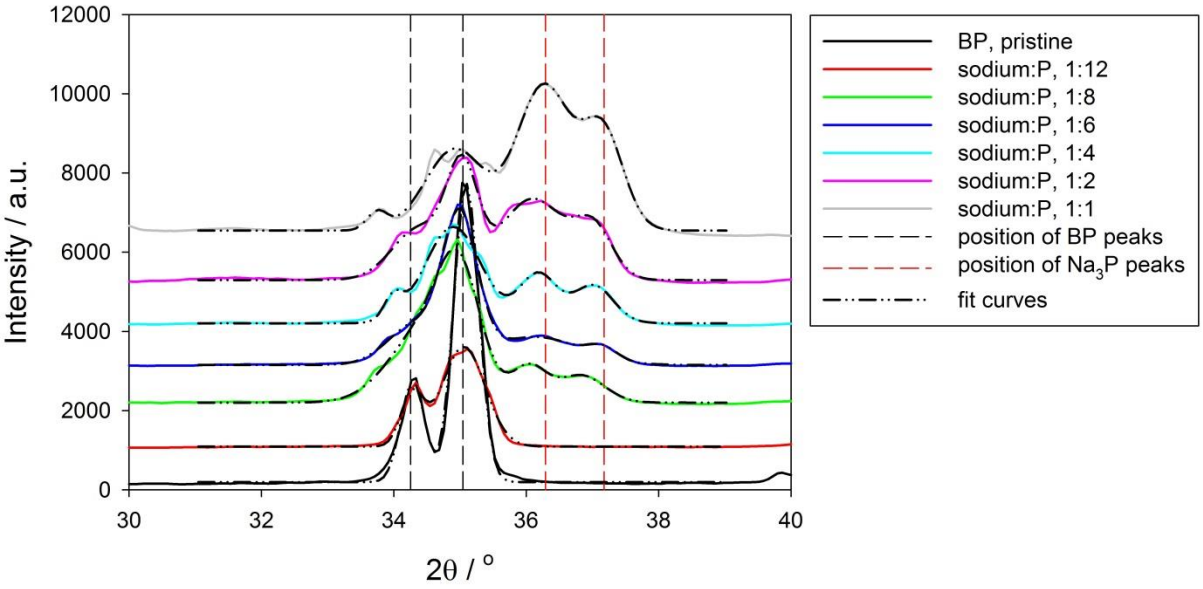

Fig. SI12: X-ray intensities for sodium@BP vs. scattering angle 2θ, with capillary and amorphous background subtracted. X-ray intensities are vertically shifted for better visibility. In this case peaks from BP and sodium@BP can easily be separated from the Na_3P peaks. From the fit curves (black dashed double dotted lines) the area of the respective peaks is calculated, which is proportional to the amount of the respective phases. From the evaluation of the relative peak areas, Fig. S16 is derived, which shows the increase of Na_3P with respect to BP.

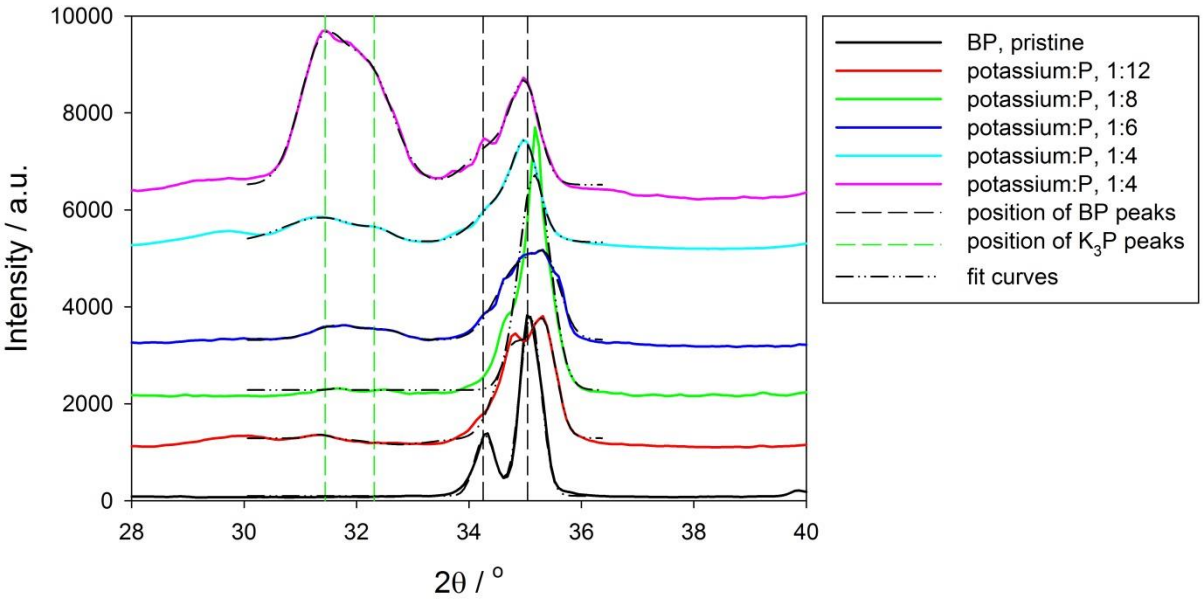

Fig. SI13: X-ray intensities for potassium@BP vs. scattering angle 2θ, with capillary and amorphous background subtracted. X-ray intensities are vertically shifted for better visibility. In this case peaks from BP and potassium@BP can easily be separated from the K_3P peaks. From the fit curves (black dashed double dotted lines) the area of the respective peaks is calculated, which is proportional to the amount of the respective phases. From the evaluation of the relative peak areas, Fig. S16 is derived, which shows the increase of K_3P with respect to BP.

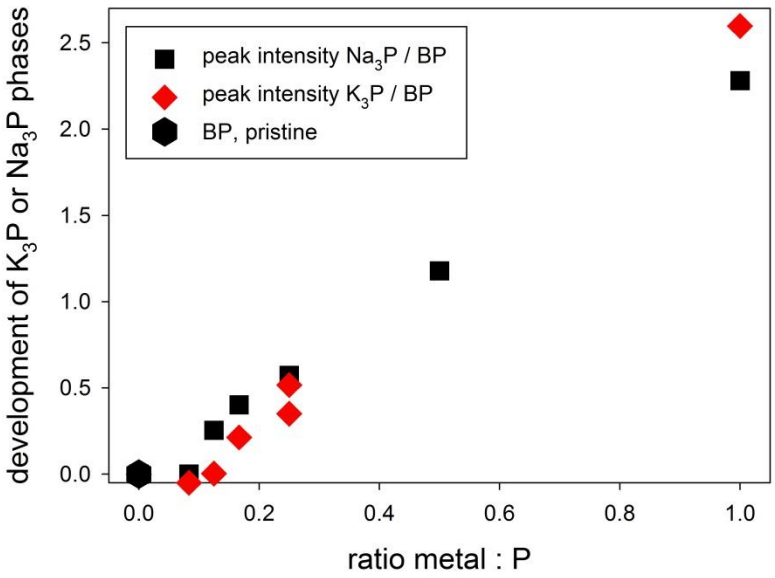

Fig. SI14: Scattering intensity of X-ray peaks from crystalline phases (Na_3P or K_3P) normalized to scattering intensities from BP peaks, indicating the relative increase of Na_3P or K_3P with respect to BP for different metal:P ratios.

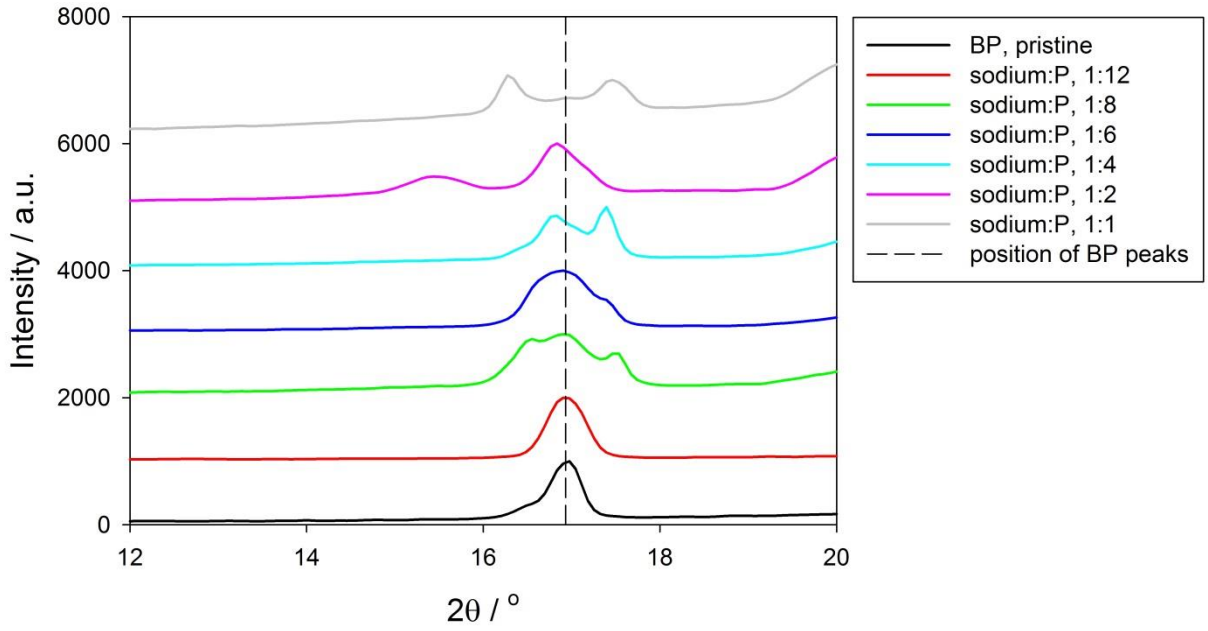

Fig. SI15: X-ray intensities for sodium@BP vs. scattering angle 2θ, with capillary and amorphous background subtracted. X-ray intensities are vertically shifted for better visibility. A peak splitting of the (002)-reflection of BP is observed, which is more pronounced the higher the metal:P ratio. These lattice distortions are described by fits with a three peaks model, corresponding to three different intercalation phases. For each phase, the lattice constant (from the respective peak maximum) and the amount of the respective phase (from the respective peak area, which is proportional to the scattering volume of each phase) is obtained.

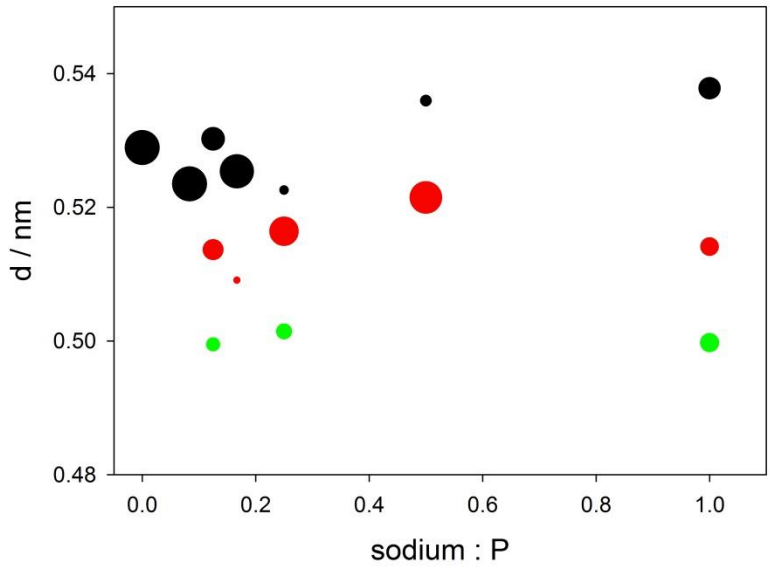

Fig. SI16: Peak maxima are converted into lattice distances from the Bragg condition $d=\lambda/(2\sin(\theta_{max}))$. Three peaks were fitted corresponding to three different lattice distances, characterized by black symbols for undistorted BP (plane distance from (002) reflection, half of the lattice constant), and red and green symbols for distorted/intercalated phases. The position indicates the lattice constant and the area of the symbol corresponds to the amount of the phase (calculated from the area of the X-ray peaks).

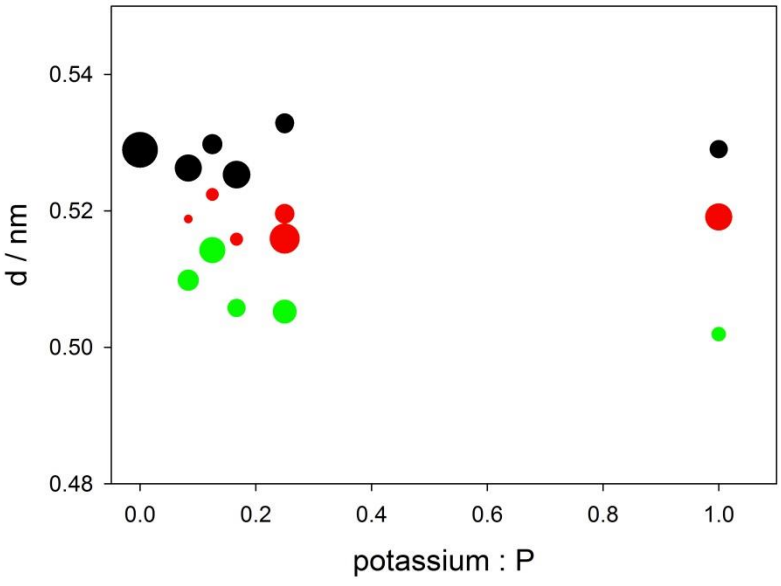

Fig. SI17: Peak maxima are converted into lattice distances from the Bragg condition $d=\lambda/(2\sin(\theta_{max}))$. Three peaks were fitted corresponding to three different lattice distances, characterized by black symbols for undistorted BP (plane distance from (002) reflection, half of the lattice constant), and red and green symbols for distorted/intercalated phases. The position indicates the lattice constant and the area of the symbol corresponds to the amount of the phase (calculated from the area of the X-ray peaks).

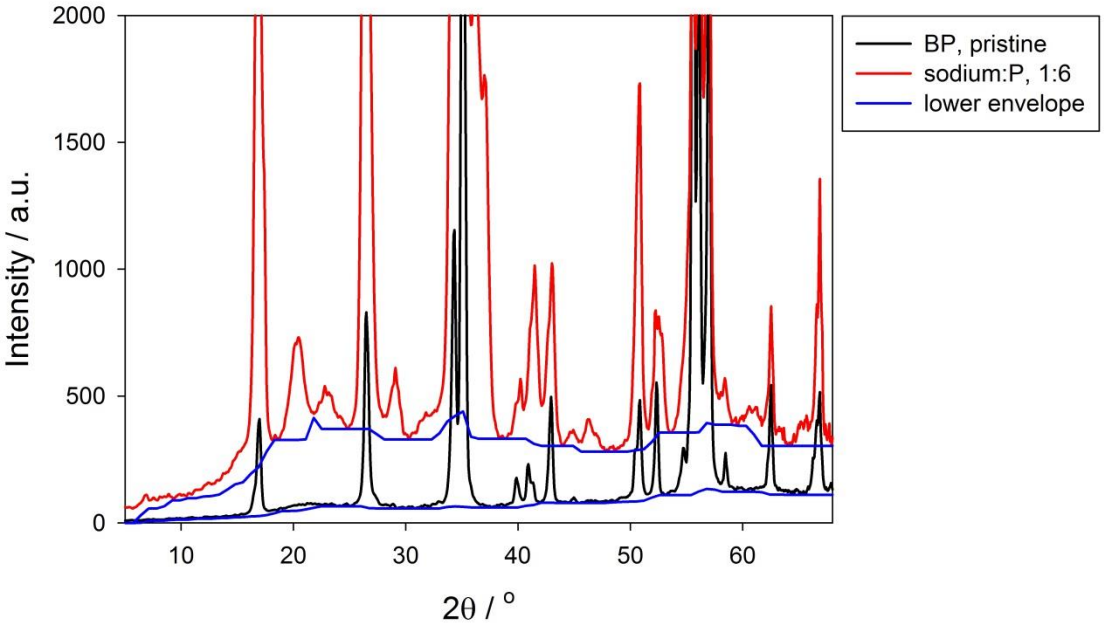

Fig. SI18: Evaluation method for crystalline to amorphous transition: From the original data (only capillary but no other background subtracted), a lower envelope was built (blue line). The X-ray intensity above the blue line corresponds to the volume of the crystalline phases (coherent scattering), the areas below the blue line to the amorphous phases (diffuse scattering).

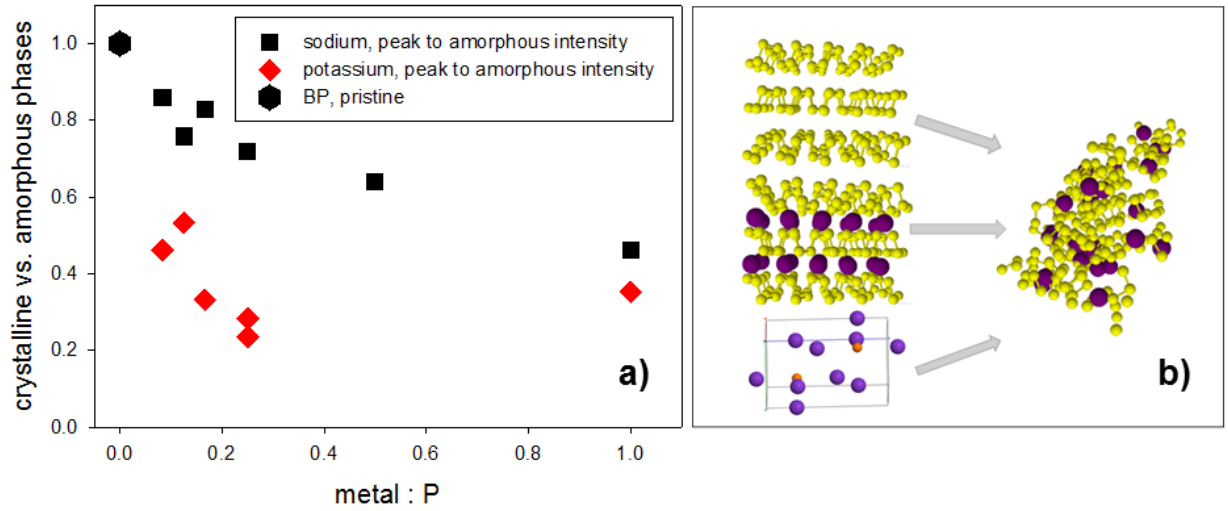

Fig. SI19: a) Decrease of scattering intensity from crystalline phases (coherent scattering) vs. amorphous scattering intensity (diffuse scattering): The symbols are calculated from the difference of crystalline (peak scattering) minus amorphous scattering intensities, normalized to the crystalline scattering intensity, i.e. $(I_{cryst} - I_{amorphous})/I_{cryst}$. The higher degree of amorphization by intercalation with the larger atom potassium is clearly visible. b) Sketch to visualize the transition from different crystalline to amorphous phases.

5. Raman spectroscopy

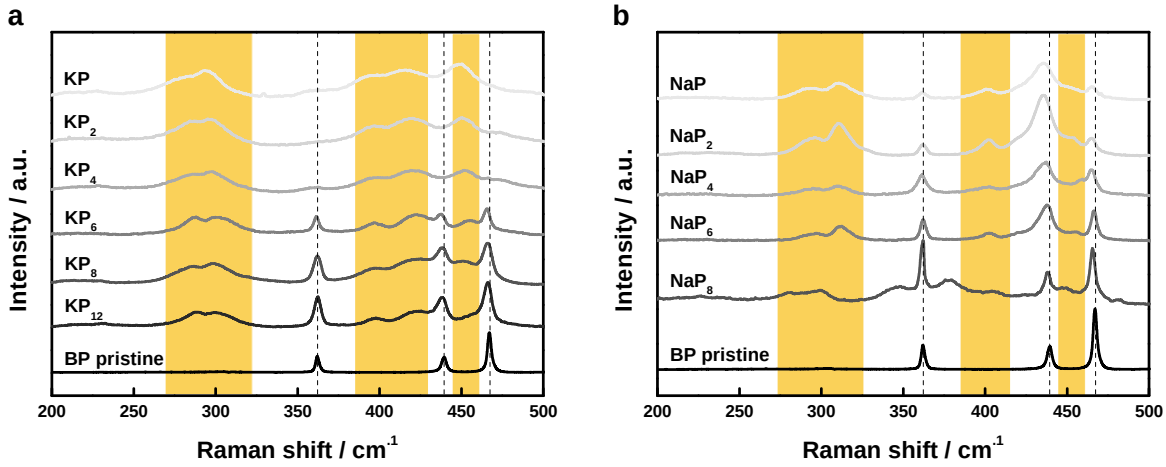

Fig. SI20: a) Mean Raman spectra of potassium BPICs prepared with different stoichiometries and measured under inert conditions. b) Mean Raman spectra of sodium BPICs prepared with different stoichiometries and measured under inert conditions. The dotted lines represent the position of the characteristic A^1_g, B_{2g} and A^2_g BP Raman modes, showing a blueshift for all the materials (see below). The areas in which the intercalation bands appear are highlighted in orange.

Raman shift development of BP vibrational modes:

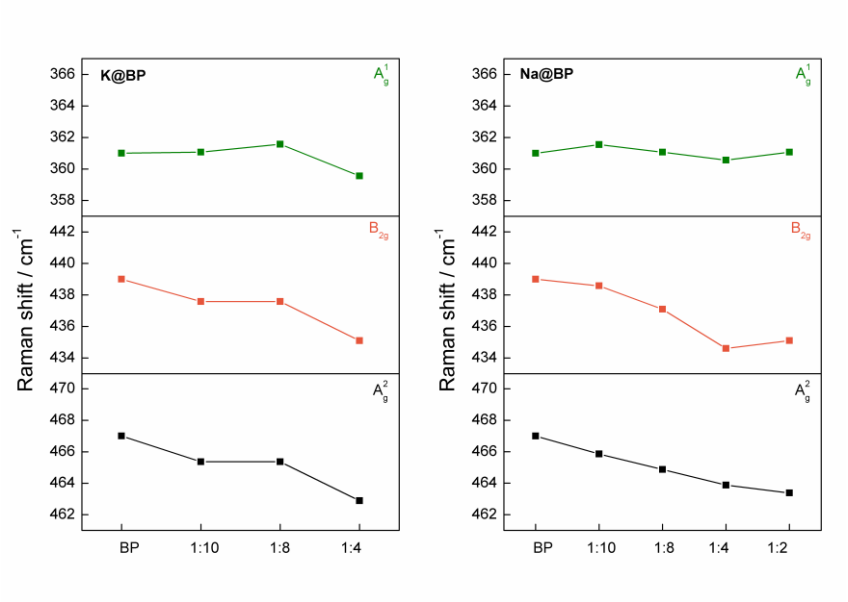

Fig. SI21: a) Raman shift analysis of selected potassium BPICs and b) the corresponding Raman shift analysis of selected sodium BPICs. The samples were stored in a glovebox several weeks after its preparation, showing similar spectra and peak shifts. The initial zero time correspond to the position of the characteristic A^1_g, B_{2g} and A^2_g BP Raman modes, showing a slight blueshift. Raman spectra were acquired in argon atmosphere (using a home-made sealed holder) on a LabRam HR Evolution confocal Raman microscope (Horiba) equipped with an automated XYZ table using 50x/0.5 LMPlan objectives. All measurements were conducted using an excitation wavelength of 532 nm, with an acquisition time of 10 s and a grating of 1800 grooves/mm. Silicon band at 521 cm^{-1} was used for calibration prior to every measurement. To minimize the photo-induced laser oxidation of the samples, the laser intensity was kept below 10 % (1.6 mW). Mean spectra were recorded using 1 μm step sizes.

Tentative Raman Peaks Assignment at the highest alkali-BP concentration:

Assignment	K@BP 1:2-1:1	/	Na@BP 1:2	/	Theory K@BP
(1) K3P	156.2	/	X	/	157.7
(2) K2P3	205.4	/	215.2	/	195.9
(3) KP2	232.8	/	232.1	/	214.9
(4) KP2	452.3	/	449.1	/	436.6
(5) KP2	499.3	/	483.0	/	481.3
X-BP *(Alkali-metal BP signature)	359.0	/	359.8	/	345.6
BP - Pristine peaks	359.0 441.1 471.3	/	359.8 435.8 463.0		(A^1_g B_{2g} A^2_g)
Intercalation peaks	278.2, 296.5	/	280.3, 299.9		
K-BP interaction peaks	392.2, 415.3	/	394.1, 410.5, 421.9		

Aging effect and influence of oxygen

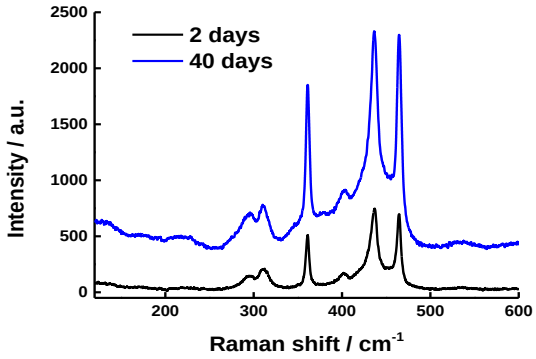

Fig. SI22: Effect of aging in the Na:BP 1:4 BPIC same sample stored 2 and 40 days, respectively.

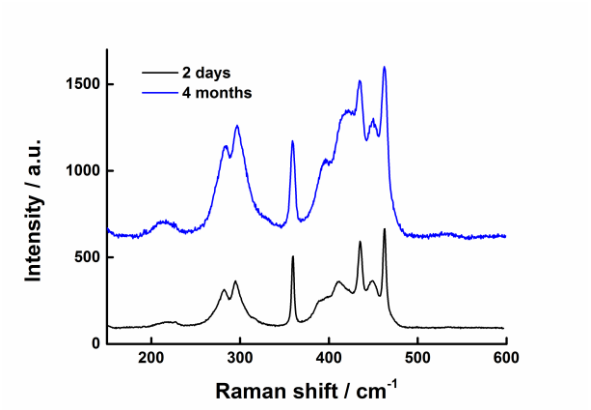

Fig. SI23: Effect of aging in the K:BP 1:4 BPIC same sample stored 2 and 4 months, respectively.

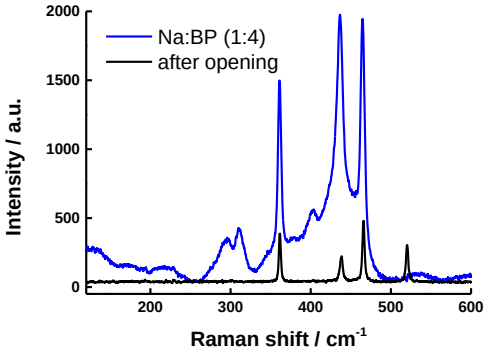

Fig. SI24: Mean Raman spectra of a Na:BP 1:4 BPIC before and after exposing the material to environmental conditions.

References:

[1] G. Kresse, J. Furthmüller *Comp. Mater. Sci.* **1996**, *6*, 15

[2] G. Kresse, J. Furthmüller *Phys. Rev. B* **1196**, *54*, 11169

[3] P. E. Blöchl, Phys. Rev. B **1994**, *50*, 17953

[4] G. Kresse, J. Joubert, Phys. Rev. B **1999**, *59*, 1758

[5] J. P. Perdew, K. Burke M. Ernzerhof *Phys. Rev. Lett.* **1996**, *77*, 3865

[6] S. Grimme, J. Antony, S. Ehrlich, H. Krieg *J. Chem. Phys.* **2010**, *132*, 154104

[7] S. Grimme, S. Ehrlich, L. Goerigk, *J. Comput. Chem.* **2011**, *32*, 1456

[8] M. Methfessel, A. T. Paxton *Phys. Rev. B* **1989**, *40*, 3616

[9] H. J. Monkhorst, J. D. Pack *Phys. Rev. B* **1976**, *13*, 5188

[10] Materials Project, http://www.materialsproject.org